Journal of Structural Geology, Vol. 7, No. 1, pp. 103 to 114, 1985
Printed in Great Britain.

0191-8141/85 $03.00 + 0.00
Pergamon Press Ltd.

Numerical modelling of finite-amplitude similar folds developing under general deformation histories

M. CASEY and P. HUGGENBERGER

Geologisches Institut der ETH, CH8092, Zurich, Switzerland

(*Received* 5 *October* 1982; *accepted in revised form* 5 *April* 1984)

Abstract—A simple model of similar folds in homogeneous materials with anisotropic properties is proposed and it is shown that the model is applicable to a wide range of natural examples of folds. A mathematical derivation is given which allows the instantaneous deformation of the folds to be calculated for any imposed bulk deformation. A means of projecting the effects of the deformation over a finite time interval is described. The modelling is illustrated by simulations of folds observed in the Morcles nappe, western Switzerland, based on the assumption that the folds formed under simple shear bulk deformation. Folds with geometrical features remarkably similar to those natural folds are produced in the modelling by varying the parameters.

INTRODUCTION

FOLDED rocks form a large proportion of orogenic belts. Strain markers can often be used to determine the finite strain at points within a fold. These strain determinations have a local significance only as they are strongly influenced by local heterogeneities within the fold. If the strain patterns associated with folds were completely understood, it would be possible to relate the local variations of strain within a fold to the strain value appropriate to the scale of a fold wavelength, which is of regional significance. Published theoretical work on fold development covers the early stages of single-layer folding (Biot 1961, Ramberg 1963) and internal buckling (Biot 1965, Cobbold *et al.* 1971). Treagus (1973) extended single-layer buckling theories to cases in which compression is oblique to the layer. The development of folds to finite amplitude has been studied using finite element analysis by, among others, Dieterich (1969) and Shimamoto & Hara (1976).

None of these approaches permits an easy modelling of the finite geometry of folds which develop in a completely general deformation. The present work seeks a solution to this problem by considering the type of fold geometry known as similar folds. The analysis is restricted to linear viscous materials. The major complexity in carrying out a mathematical analysis of folding arises from the fact that two-dimensional analyses are usually required to describe the folding processes. This paper shows that in the case of similar folding, the analysis can be reduced to a one-dimensional problem. It is a generalization of the approach of Cobbold (1976) and similar to that of Bayly (1964), except that the latter author related the deformation in the folds to the stress at the boundary rather than to the imposed bulk deformation. An outline of the analysis is given here, only matters relevant to the modelling of fold patterns being described in detail. A detailed analysis and implications for the mechanics of folding will be given elsewhere.

SIMILAR FOLDING IN A GENERAL IMPOSED STRAIN

An idealization of similar folding

Most natural folds occur in multilayered sequences of alternating layers differing in competence. The geometry of the structure changes markedly from the more competent to the less competent layers but the average geometry over several layers frequently approximates the similar-fold model (Ramsay 1967). A multilayered sequence of more and less competent layers has rheological properties on the large scale identical to those of transversely isotropic materials (Biot 1965, Cobbold *et al.* 1971). That is, the material is hard to deform when the principal incremental strain axes are parallel and perpendicular to the layering and easier to deform when the strain axes are at 45° to the layering. In the latter case the imposed strain can be taken up by shear deformation in the less competent layers.

The following assumptions are made for the subsequent analysis.

(1) The material in which the folds develop is anisotropic and homogeneous.
(2) The material has linear viscous rheological properties.
(3) The geometry of the similar folds is idealized as shown in Fig. 1, where the coordinate systems used are also shown.
(4) The inflexion points are axes of two-fold rotational symmetry.
(5) The points of two-fold rotational symmetry move at velocities determined by the imposed deformation.

In Fig. 1 the line joining the inflexion points of successive layers has been set parallel to the y axis of the fold reference system x,y. Assumption 5 means that the y component of the strain-rate $\dot{e}_y$ in the x,y system is determined by the imposed deformation.

The coordinate system x',y' of Fig. 1 is the main

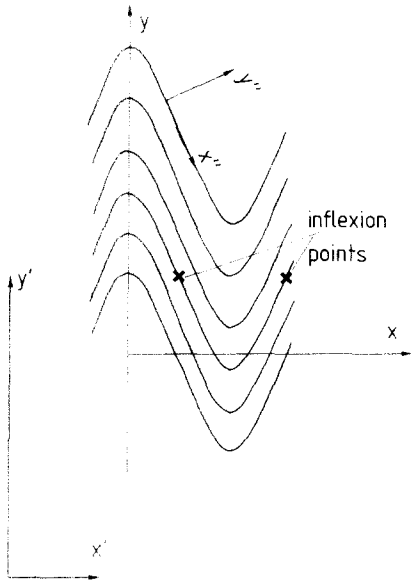

Fig. 1. Idealized similar fold geometry and coordinate systems used. The x',y' system is the general reference system in which the imposed bulk deformation and the fold geometry are given. The system x,y is set up with the y axis parallel to the axial planes of the folds. The system x'',y'' has x'' parallel to the folded surfaces and is used in the definition of the relation between stress and strain rate.

reference system in which the imposed bulk deformation is specified. In general x,y and x',y' are not parallel as shown in Fig. 1.

Conditions on the variation of stress and strain-rate across an ideal similar fold

The imposed deformation is given as the velocity gradient matrix in the x',y' system

$$v'_{k,l} = \begin{pmatrix} \frac{\partial v'_{x'}}{\partial x} & \frac{\partial v'_{x'}}{\partial y} \\ \frac{\partial v'_{y'}}{\partial x} & \frac{\partial v'_{y'}}{\partial y} \end{pmatrix}. \tag{1}$$

The strain-rates and rotation rates are related to the components of the velocity gradient matrix by the following equations

$$\begin{aligned} \dot{e}_{x'} &= \frac{\partial v'_{x'}}{\partial x'} \\ \dot{e}_{y'} &= \frac{\partial v'_{y'}}{\partial y'} \\ \dot{\gamma}_{x'y'} &= \frac{\partial v'_{x'}}{\partial y'} + \frac{\partial v'_{y'}}{\partial x'} \\ \omega &= \frac{1}{2}\left(\frac{\partial v'_{x'}}{\partial y'} - \frac{\partial v'_{y'}}{\partial x'}\right). \end{aligned} \tag{2}$$

The above equations can be easily inverted to give equations relating the components of the velocity gradient matrix to the strain-rate and rotation-rate terms.

Stress equilibrium and strain compatibility can be used to find constraints on the variations of stress and strain-rate across the folds. The reference system of Fig. 1 was set up with the y axis in the direction in which fold profile geometry remains constant. If the geometry is to remain constant in the y direction the components of stress and of the velocity gradient matrix must not vary with y. Velocity components may, however, vary linearly with y. This means that differentiation of stress and velocity gradient terms with respect to y gives a result that can be set to zero. This analysis has been carried out by Cobbold (1976) for symmetric similar folds but the results for strain variation must be generalized to cover the current cases.

The stress equilibrium equations are

$$\frac{\partial \sigma_x}{\partial x} + \frac{\partial \tau_{xy}}{\partial y} = 0 \tag{3}$$

$$\frac{\partial \tau_{xy}}{\partial x} + \frac{\partial \sigma_y}{\partial y} = 0. \tag{4}$$

Or, using the fact that differentiation with respect to y gives zero

$$\frac{\partial \sigma_x}{\partial x} = 0 \tag{5}$$

$$\frac{\partial \tau_{xy}}{\partial x} = 0. \tag{6}$$

Equations (5) and (6) express the condition that σ_x and τ_{xy} are constant across the fold profile.

Differentiating the terms in the first column of the velocity gradient matrix in (1) with respect to y and setting the result equal to zero gives

$$\frac{\partial^2 v_x}{\partial y\, \partial x} = 0 \tag{7}$$

$$\frac{\partial^2 v_y}{\partial y\, \partial x} = 0. \tag{8}$$

Using the fact that the order of partial differentiation does not influence the result

$$\frac{\partial}{\partial x}\left(\frac{\partial v_x}{\partial y}\right) = 0 \tag{9}$$

$$\frac{\partial}{\partial x}\left(\frac{\partial v_y}{\partial y}\right) = \frac{\partial \dot{e}_y}{\partial x} = 0. \tag{10}$$

Equation (10) shows that $\dot{e}_y$ is constant across the fold profile and equations (9) and (10) show that the second column of the velocity gradient matrix is constant across the profile. This means that the instantaneous straining of the fold can only differ from the imposed deformation in the first column of the velocity gradient matrix. A variation of $\partial v_y/\partial x$ corresponds to a heterogeneous simple shearing with shear planes parallel to y. See also Cobbold (1976) equation (32).

The strain-rate stress relation for anisotropic linear viscous materials

The material in which the folds develop is homogeneous but has anisotropic deformation properties. The

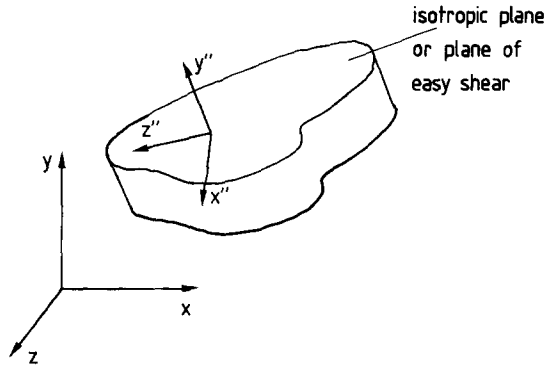

Fig. 2. Representation of an anisotropic material. The stress strain rate relation is defined in coordinate system x'',y'',z''.

lines defining the folds are directions parallel to which shearing deformation is easiest. The material is transversely isotropic (Zienkiewicz 1971, p. 55) or orthotropic (Biot 1965, Cobbold *et al.* 1971, Cobbold 1976) and is shown in Fig. 2.

In the plane of the stratification (the x'' z'' plane of Fig. 2) the material has isotropic properties. That is, the values of the parameters relating stress and strain-rate do not vary with the orientation of the coordinate axes in the plane of stratification. For this reason the plane of stratification is called the isotropic plane.

In the coordinate system x'',y'',z'' of Fig. 2 the deformation rates and stress are related by

$$\begin{aligned}
\dot{e}_{x''} &= \frac{\sigma_{x''}}{\eta_1} - \nu_2 \frac{\sigma_{y''}}{\eta_2} - \nu_1 \frac{\sigma_{z''}}{\eta_1} \\
\dot{e}_{y''} &= \nu_2 \frac{\sigma_{x''}}{\eta_2} + \frac{\sigma_{y''}}{\eta_2} - \nu_2 \frac{\sigma_{z''}}{\eta_2} \\
\dot{e}_{z''} &= -\nu_1 \frac{\sigma_{x''}}{\eta_1} - \nu_2 \frac{\sigma_{y''}}{\eta_2} + \frac{\sigma_{z''}}{\eta_1} \\
\dot{\gamma}_{x''z''} &= 2(1+\nu_1)/\eta_1 \, \tau_{x''z''} \\
\dot{\gamma}_{y''z''} &= \frac{1}{G_2} \tau_{x''y''} \\
\dot{\gamma}_{y''z''} &= \frac{1}{G_2} \tau_{y''z''}.
\end{aligned} \tag{11}$$

These equations were adapted from the equations for anisotropic elasticity given in Zienkiewicz (1971, p. 55). η_1 is the direct viscosity modulus and ν_1 the equivalent to Poisson's ratio in the isotropic plane, $x''z''$. η_2, G_2 and ν_2 are the direct modulus, shear modulus and Poisson's ratio equivalent, respectively in the planes containing the normal to the isotropic plane.

Strain-rate components $\dot{e}_{z''}$, $\dot{\gamma}_{x''z''}$ and $\dot{\gamma}_{y''z''}$ are all zero for plane strain. Using the condition that $\dot{e}_{z''}$ is zero to eliminate $\sigma_{z''}$ and putting $\eta_1/\eta_2 = n$ and $G_2/\eta_2 = m$ gives

$$[D''] = \begin{bmatrix} \frac{1}{n\eta_2}(1-\nu_1^2) & -\frac{\nu_2}{\eta_2}(1+\nu_1) & 0 \\ \frac{-\nu_2}{\eta_2}(1+\nu_2 & \frac{1}{\eta_2}(1-n\nu_2^2) & 0 \\ 0 & 0 & \frac{1}{m\eta_2} \end{bmatrix} \tag{12}$$

where $[D'']$ is the strain-rate stress matrix in the system x'', y''.

This way of defining the strain-rate stress equation uses five moduli to define the behaviour and differs from the analysis of Cobbold (1976) who employed two (N, the direct modulus and Q, the shear modulus) because he considered incompressible materials in plane strain. Equation (12) permits volume change (ν_1 and $\nu_2 \neq 0.5$) and different direct moduli ($n \neq 1.0$). The parameter n is always set to 1.0 in the present application. The parameter m defines the degree of anisotropy; a value of $\frac{1}{3}$ corresponds to isotropic behaviour and $m < \frac{1}{3}$ gives easy shear into the isotropic plane (Fig. 2).

The strain-rate stress relation for an anisotropic material is different in differently oriented coordinate systems and equation (12) applies for systems with the y axis normal to the plane of easy shear only. In the following paragraphs a means of transforming the matrix $[D]$ to other coordinate systems is derived.

Stress components can be transformed from x, y to another system x'', y'' which is rotated an angle β (anticlockwise positive) from x,y by using

$$[\sigma''] = [T][\sigma] \tag{13}$$

where $[T]$ is given by

$$[T] = \begin{bmatrix} \cos^2\beta & \sin^2\beta & 2\sin\beta\cos\beta \\ \sin^2\beta & \cos^2\beta & -2\sin\beta\cos\beta \\ -\sin\beta\cos\beta & \sin\beta\cos\beta & \cos^2\beta - \sin^2\beta \end{bmatrix}. \tag{14}$$

The matrix $[T]$ can also be used to transform the matrix $[D]$ from a local system with x'' parallel to the layering at a point in the fold to the fold reference system x, y, (Fig. 1). In the x'', y'' system the stress $[\sigma'']$ and strain-rates $[\dot{e}'']$ do work at a rate given by

$$W = [\sigma'']^{\mathrm{T}}[\dot{e}'']. \tag{15}$$

Here, the superscript T denotes the transpose of the matrix or vector concerned. The stress $[\sigma]$ and strain-rates $[\dot{e}]$ in the unprimed system do an equal amount of work, since the deformation is the same.

$$[\sigma'']^{\mathrm{T}}[\dot{e}''] = [\sigma]^{\mathrm{T}}[\dot{e}]$$

or,

$$[\sigma'']^{\mathrm{T}}[D''][\sigma''] = [\sigma]^{\mathrm{T}}[D][\sigma].$$

Using (13)

$$[\sigma]^{\mathrm{T}}[T]^{\mathrm{T}}[D''][T][\sigma] = [\sigma]^{\mathrm{T}}[D][\sigma].$$

Therefore

$$[D] = [T]^{\mathrm{T}}[D''][T]. \tag{16}$$

This general strain-rate stress matrix has no zero elements, in contrast to $[D'']$ in (12).

Writing the general strain-rate stress relation in full

$$\begin{bmatrix} \dot{e}_x \\ \dot{e}_y \\ \dot{\gamma}_{xy} \end{bmatrix} = \begin{bmatrix} d_{11} & d_{12} & d_{13} \\ d_{12} & d_{22} & d_{23} \\ d_{13} & d_{23} & d_{33} \end{bmatrix} \begin{matrix} \sigma_x \\ \sigma_y \\ \tau_{xy}. \end{matrix} \tag{17}$$

The d_{ij} terms stand for the matrix $[D]$ and, as is indicated by the indexing, the $[D]$ matrix is symmetric.

Analysis of similar folding

In equation (17) $\dot{e}_y$, σ_x and τ_{xy} are constant across the fold profile. The other terms, ($\dot{e}_x$, $\dot{\gamma}_{xy}$, σ_y and the d_{ij}) vary according to the orientation of the plane of easy shear. To emphasize the difference between stress and strain terms which vary in x and those which are constant, the former will be written with x in parentheses, for example $\dot{\gamma}_{xy}(x)$.

From (17)

$$\dot{e}_y = d_{12}\sigma_x + d_{22}\sigma_y(x) + d_{23}\tau_{xy}.$$

Solving for $\sigma_y(x)$

$$\sigma_y(x) = \frac{\dot{e}_y}{d_{22}} - \frac{d_{12}}{d_{22}}\sigma_x - \frac{d_{23}}{d_{22}}\tau_{xy}. \tag{18}$$

This expression for $\sigma_y(x)$ can be substituted into equation (17) to give equations relating the variable strain-rate components to $\dot{e}_y$, which is known, and σ_x and τ_{xy}, which are constant

$$\dot{e}_x(x) = \left(d_{11} - \frac{d_{12}^2}{d_{22}}\right)\sigma_x + \left(d_{13} - \frac{d_{23}d_{12}}{d_{22}}\right)\tau_{xy} + \frac{d_{12}}{d_{22}}\dot{e}_y \tag{19}$$

$$\dot{\gamma}_{xy}(x) = \left(d_{13} - \frac{d_{23}d_{12}}{d_{22}}\right)\sigma_x + \left(d_{33} - \frac{d_{23}^2}{d_{22}}\right)\tau_{xy} + \frac{d_{23}}{d_{22}}\dot{e}_y. \tag{20}$$

The values of σ_x and τ_{xy} are not known at the start of the analysis, but once they are known the strain-rate across the profile can be calculated using equations (19) and (20).

From assumption 5, the velocity at the inflexion points is known. The origin is located at an inflexion point on one limb (Fig. 3). The velocity at the origin is set to zero. The velocity at a point x^* on the x axis is given by integrating the velocity gradient terms along the line $y = 0$, (Fig. 3).

$$v_x(x^*,0) = \int_0^{x^*} \frac{\partial v_x}{\partial x}\,dx = \int_0^{x^*} \dot{e}_x\,dx$$

$$v_y(x^*,0) = \int_0^{x^*} \frac{\partial v_y}{\partial x}\,dx.$$

From the definitions of strain-rates in (2)

$$\frac{\partial v_y}{\partial x} = 1/2\dot{\gamma}_{xy} + \omega \tag{21}$$

$$\frac{\partial v_x}{\partial y} = 1/2\dot{\gamma}_{xy} - \omega. \tag{22}$$

From equation (7), $\partial v_x/\partial y$ is constant across the fold, and

$$\frac{\partial v_y}{\partial x} = \dot{\gamma}_{xy} - \frac{\partial v_x}{\partial y} \tag{23}$$

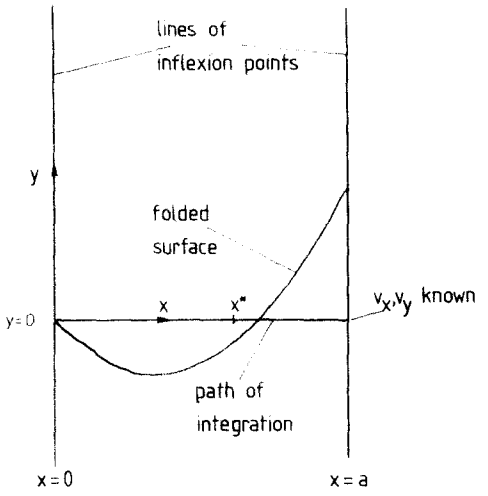

Fig. 3. The velocities at the inflexion points are known and the velocities of points across the fold may be obtained by integration of velocity gradient terms along the x axis. The velocities of points on the folded surface differ from those on the x axis.

enables $\partial v_y/\partial x$ to be related to known quantities.

Thus

$$v_x(x^*,0) = \int_0^{x^*} \dot{e}_x\,dx \tag{24}$$

$$v_y(x^*,0) = \int_0^{x^*} \left(\dot{\gamma}_{xy} - \frac{\partial v_x}{\partial y}\right)dx. \tag{25}$$

Substituting for $\dot{e}_x$ and $\dot{\gamma}_{xy}$ from (19) and (20)

$$v_x(x^*,0) = \int_0^{x^*} \left[\left(d_{11} - \frac{d_{12}^2}{d_{22}}\right)\sigma_x + \left(d_{13} - \frac{d_{23}d_{12}}{d_{22}}\right)\tau_{xy} + \frac{d_{12}}{d_{22}}\dot{e}_y\right]dx \tag{26}$$

$$v_y(x^*,0) = \int_0^{x^*} \left[\left(d_{13} - \frac{d_{23}d_{12}}{d_{22}}\right)\sigma_x + \left(d_{33} - \frac{d_{23}^2}{d_{22}}\right)\tau_{xy} + \frac{d_{23}}{d_{22}}\dot{e}_y - \frac{\partial v_x}{\partial y}\right]dx. \tag{27}$$

If the integrals in equations (24) and (25) are taken to the inflexion point on the next fold limb ($x^* = a$) then the velocities are known, using assumption 5

$$\frac{\partial v_x}{\partial x}a = \sigma_x\int_0^a \left(d_{11} - \frac{d_{12}^2}{d_{22}}\right)dx + \tau_{xy}\int_0^a \left(d_{13} - \frac{d_{23}d_{12}}{d_{22}}\right)dx + \dot{e}_y\int_0^a \frac{d_{12}}{d_{22}}\,dx \tag{28}$$

$$\frac{\partial v_y}{\partial x}a = \sigma_x\int_0^a \left(d_{13} - \frac{d_{23}d_{12}}{d_{22}}\right)dx + \tau_{xy}\int_0^a \left(d_{33} - \frac{d_{23}^2}{d_{22}}\right)dx + \dot{e}_y\int_0^a \frac{d_{23}}{d_{22}}\,dx - \frac{\partial v_x}{\partial y}a. \tag{29}$$

The terms $\dot{e}_y$, σ_x and τ_{xy} are constant across the fold and have been taken outside the integrals.

Rearranging and putting

$$\gamma_{xy} = \frac{\partial v_y}{\partial y} + \frac{\partial v_y}{\partial x}$$

$$\sigma_x \int_0^a \left(d_{11} - \frac{d_{12}^2}{d_{22}}\right) dx + \tau_{xy} \int_0^a \left(d_{13} - \frac{d_{13}d_{12}}{d_{22}}\right) dx = a\,\dot{e}_x - \dot{e}_y \int_0^a \frac{d_{12}}{d_{22}}\,dx \tag{30}$$

$$\sigma_x \int_0^a \left(d_{13} - \frac{d_{23}d_{12}}{d_{22}}\right) dx + \tau_{xy} \int_0^a \left(d_{33} - \frac{d_{23}^2}{d_{22}}\right) dx = a\,\dot{\gamma}_{xy} - \dot{e}_y \int_0^a \frac{d_{23}}{d_{22}}\,dx. \tag{31}$$

Equations (30) and (31) represent two simultaneous equations for σ_x and τ_{xy}. The integrals involve terms of the strain-rate stress matrix $[D]$ which vary according to the orientation of the plane of easy shear. For a given fold shape, the integrals can be evaluated numerically and the equations can be solved for σ_x and τ_{xy}. Note that the rigid rotation rate, ω, of the applied deformation has no influence on the stress at the instant considered. Equations (30) and (31) can also be derived by minimizing the rate of dissipation of energy within a strip of material running from one line of inflexion points to the next and the work done by forces acting on the boundaries of the strip.

Once σ_x and τ_{xy} have been found, equations (18–20) can be used to give the other stress and strain-rate components across the fold. The diagonal components of the velocity gradient matrix are $\dot{e}_x$ and $\dot{e}_y$, $\partial v_x/\partial y$ is constant and equal to the imposed value (equation 9), and $\partial v_y/\partial x$ can be obtained from equation (23). Equations (26) and (27) can be used to obtain the velocity of points across the fold along the line $y = 0$. To obtain the velocity along the surface defining the fold (Fig. 3) a quantity must be added to both components to take account of the homogeneous strain-rate

$$v_x(x,y) = v_x(x,0) + \tfrac{1}{2}\dot{\gamma}_{xy}\,y$$
$$v_y(x,y) = v_y(x,0) + \dot{e}_y\,y. \tag{32}$$

The distribution of deformation between competent and incompetent units

The homogeneous material with anisotropic deformation properties is used to approximate an alternating sequence of isotropic layers of different viscosity. The velocity gradient matrix calculated above can be applied to a multilayered model at various points across the fold to calculate the velocity gradient matrix in each of the constituent layers.

In this analysis it is assumed that the strain in each unit is homogeneous. Effects in real folds, such as the squeezing of incompetent units into the fold hinges (Williams 1980), and heterogeneities associated with the fold hinge are ignored. Thus this part of the analysis is applicable only to regions of the fold away from the hinge where the beds are straight.

This analysis represents a sub-problem independent of the analysis in the previous sections.

A multilayered packet consisting of layers of viscosities η_1 and η_2 and relative thicknesses F and (1-F) is shown in Fig. 4. The bedding planes have been set parallel to y'' so that continuity conditions obtained above (equations 5, 6, 9 and 10) can be applied directly. Points on the centre lines of the layers are points of twofold rotational symmetry, and assumption 5 is applied here in the same way as for fold inflexion points; that is, velocities of points on the centre lines of the layers are given by the imposed deformation

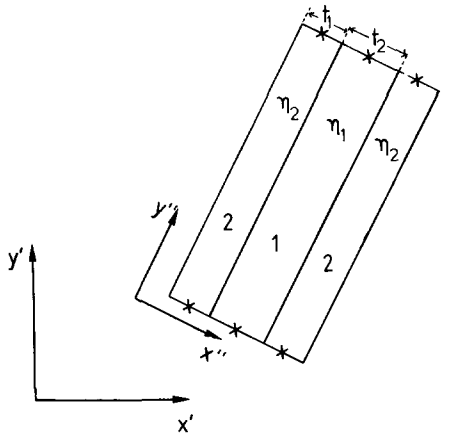

Fig. 4. A multilayer sequence of alternating layers of viscosities η_1 and η_2 and thicknesses t_1 and t_2.

$$\begin{bmatrix} {}^i\sigma_{x''} \\ {}^i\sigma_{y''} \\ {}^i\tau_{x''y''} \end{bmatrix} = \begin{bmatrix} {}^ic_{11} & {}^ic_{12} & 0 \\ {}^ic_{12} & {}^ic_{22} & 0 \\ 0 & 0 & {}^ic_{33} \end{bmatrix} \begin{bmatrix} {}^ie_{x''} \\ {}^ie_{y''} \\ {}^i\gamma_{x''y''} \end{bmatrix}. \tag{33}$$

The matrix c_{ij} is given by

$$c_{ij} = \frac{\eta(1-\nu)}{(1+\nu)(1-2\nu)} \times \begin{bmatrix} 1 & \nu/(1-\nu) & 0 \\ \nu/(1-\nu) & 1 & 0 \\ 0 & 0 & (1-2\nu)/2(1-\nu) \end{bmatrix},$$

where η is the direct viscosity modulus and ν is a modulus equivalent to Poisson's ratio. This equation was taken from Zienkiewicz (1971, p. 54, equation 4.20).

The conditions for stress variation, equations (5) and (6), give

$${}^1\sigma_{x''} = {}^2\sigma_{x''} \tag{34}$$

$${}^1\tau_{x''y''} = {}^2\tau_{x''y''}. \tag{35}$$

The conditions on the components of the velocity gradient matrix, equations (9) and (10, give

$${}^1\dot{e}_{y''} = {}^2\dot{e}_{y''} = {}^1\dot{e}_{y''} \tag{36}$$

$$\frac{{}^1\partial v_{x''}}{\partial y''} = \frac{{}^2\partial v_{x''}}{\partial y''} = \frac{{}^1\partial v_{x''}}{\partial y''}. \tag{37}$$

The continuity of shear stress allows an equation relating shear strain-rate in the two layers to be written

$${}^1\dot{\gamma}_{x''y''} = \frac{{}^2c_{33}}{{}^1c_{33}}\,{}^2\dot{\gamma}_{x''y''}. \tag{38}$$

Writing out the first of equations (33) for each layer and equating according to equation (34) gives

$$^{1}c_{11}{}^{1}\dot{e}_{x''} + {}^{1}c_{12}{}^{1}\dot{e}_{y''} = {}^{2}c_{11}{}^{2}\dot{e}_{x''} + {}^{2}c_{12}{}^{2}\dot{e}_{y''}. \quad (39)$$

Using equation (36) and rearranging:

$$^{1}\dot{e}_{x''} = \frac{{}^{2}c_{11}{}^{2}\dot{e}_{x''} + ({}^{2}c_{12} - {}^{1}c_{12})\,{}^{1}\dot{e}_{y''}}{{}^{1}c_{11}}. \quad (40)$$

From considerations of the x component of velocity it can be shown that

$$^{1}\dot{e}_{x''} = F\,{}^{1}\dot{e}_{x''} + (1-F)\,{}^{2}\dot{e}_{x''} \quad (41)$$

Eliminating $^{1}\dot{e}_{x''}$ between (40) and (41) gives an equation relating $^{2}\dot{e}_{x''}$ to known quantities

$$^{2}\dot{e}_{x''} = \frac{{}^{2}c_{11}{}^{1}\dot{e}_{x''} - ({}^{2}c_{12} - {}^{1}c_{12})\,F\,{}^{1}\dot{e}_{y''}}{{}^{2}c_{11}F + {}^{1}c_{11}(1-F)}. \quad (42)$$

From equations (22) and (37):

$$\frac{1}{2}\,{}^{1}\dot{\gamma}_{x''y''} - {}^{1}\omega = \frac{1}{2}\,{}^{2}\dot{\gamma}_{x''y''} - {}^{2}\omega = \frac{{}^{1}\partial v_{x''}}{\partial y''}.$$

Thus:

$$^{1}\omega = \frac{1}{2}\,{}^{1}\dot{\gamma}_{x''y''} - \frac{{}^{1}\partial v_{x''}}{\partial y''} \quad (43)$$

and

$$^{2}\omega = \frac{1}{2}\,{}^{2}\dot{\gamma}_{x''y''} - \frac{{}^{1}\partial v_{x''}}{\partial y''}. \quad (44)$$

From considerations of the y component of velocity

$$F\frac{{}^{1}\partial v_{y''}}{\partial x''} + (1-F)\frac{{}^{2}\partial v_{y''}}{\partial x''} = \frac{{}^{1}\partial v_{y''}}{\partial x''}. \quad (45)$$

Using equation (21)

$$F(\tfrac{1}{2}\,{}^{1}\dot{\gamma}_{x''y''} + {}^{1}\omega) + (1-F)(\tfrac{1}{2}\,{}^{2}\dot{\gamma}_{x''y''} + {}^{2}\omega) = \frac{{}^{1}\partial v_{y''}}{\partial x''}. \quad (46)$$

Using equations (43) and (44) to eliminate $^{1}\omega$ and $^{2}\omega$ and rearranging

$$F\,{}^{1}\dot{\gamma}_{x''y''} + (1-F)\,{}^{2}\dot{\gamma}_{x''y''} = \frac{{}^{1}\partial v_{x''}}{\partial y''} + \frac{{}^{1}\partial v_{y''}}{\partial x''} = {}^{1}\dot{\gamma}_{x''y''}. \quad (47)$$

Using (38) to eliminate $^{1}\dot{\gamma}_{x''y''}$ gives

$$^{2}\dot{\gamma}_{x''y''} = \frac{{}^{1}\dot{\gamma}_{x''y''}}{F\dfrac{{}^{2}c_{33}}{{}^{1}c_{33}} + (1-F)}. \quad (48)$$

From these equations the strain-rate and rotation rate terms of the component layers of the multilayer sequence can be calculated once their relative thicknesses and viscosities have been assigned. The velocity gradient matrices can be obtained from the strain-rate and rotation rates, the diagonal terms being $e_{x''}$ and $e_{y''}$ and the off-diagonal elements are given by equations (21) and (22).

KINEMATICS AND TIME INTEGRATION

The geometry of the first-formed folds is specified by giving the coordinates of points at intervals across the profile and the direction in which the fold geometry is constant, which is also parallel to the line joining inflexion points on successive layers. The geometry of the folds at later times is given by the coordinates of the chosen points. The line joining the inflexion points is reoriented by the deformation gradient matrix defining the bulk finite deformation. The geometry at time t is shown in Fig. 5. The analysis presented above for the calculation of the velocities across the fold along the line $y = 0$ requires as input, the orientation of the direction of easy shear at points across the fold profile and the imposed strain matrix. The orientation of the line of easy shear is obtained from the slope of the fold profile. The strain-rates and rotation rates are calculated from the imposed velocity gradient matrix by equations (2).

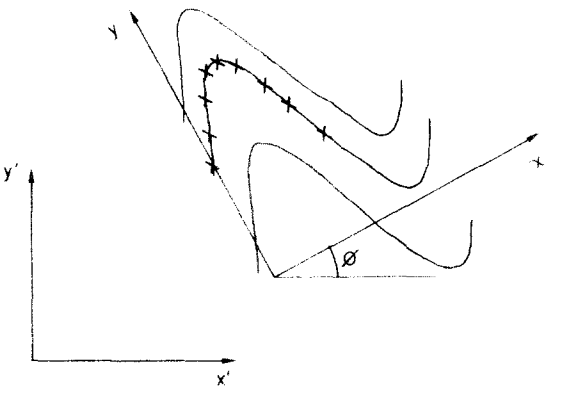

Fig. 5. The geometry of the model at some time during the simulation. The symbol X represents the points used to define the fold profile shape. The angle ϕ gives the orientation of the axial plane relative to the general reference system x',y'.

A difficulty in this analysis is that the fold coordinate system x, y is rotating relative to the general reference frame x', y' and this rotation has to be taken into account in transforming the velocity gradient matrix, rotation rates and velocities but not strain-rates and coordinates (see Eringen 1962, pp. 89–93). This problem can be obviated here, as rigid rotations do not affect the instantaneous mechanics of the buckling instability and the contribution to the velocity from the strain rates and the rigid rotations of the imposed deformation can be considered separately and added to give the final value.

At any instant the velocity of the points on the fold profile which represent the geometry is a function of the coordinates of the points and of the bulk finite deformation gradient matrix $\left[\begin{smallmatrix} a & b \\ c & d \end{smallmatrix}\right]$

$$v' = v'(x',a,b,c,d),$$

where v' and x' represent the vector formed of all the x' and y' components of the velocities and coordinates of the points in the fold used to represent the geometry.

The velocities are also the time rate of change of position, hence:

$$\frac{dx'}{dt} = \frac{dx'}{dt}\,(x',a,b,c,d).$$

Thus the projection through time involves the solution of a system of ordinary differential equations, which in

this case was achieved by the fourth order Runge–Kutta method (Ralston & Wilf 1960, ch. 9).

The time rate of change of the deformation gradient matrix is given by equation (49), which was adapted from Eringen (1967, p. 70 equation 2.4.1)

$$\begin{aligned}
\frac{da}{dt} &= \frac{\partial v_x}{\partial x}\,a + \frac{\partial v_x}{\partial y}\,c \\
\frac{db}{dt} &= \frac{\partial v_x}{\partial x}\,b + \frac{\partial v_x}{\partial y}\,d \\
\frac{dc}{dt} &= \frac{\partial v_y}{\partial x}\,a + \frac{\partial v_y}{\partial y}\,c \\
\frac{dd}{dt} &= \frac{\partial v_y}{\partial x}\,b + \frac{\partial v_y}{\partial y}\,d.
\end{aligned} \tag{49}$$

This also represents a system of ordinary differential equations which must be solved simultaneously with those for the points defining the fold profile by the same method.

The deformation gradient matrices defining the finite imposed deformation and the finite deformation in the component layers of the multilayer were all calculated in this way. The usual measures of finite strain, elongations, principal directions and finite rigid rotation can be calculated from the deformation gradient matrix using equations (7)–(10) of Ramsay & Graham (1970).

THE VALIDITY OF THE ASSUMPTIONS AND THE APPLICABILITY OF THE MODEL

Assumptions must be made before any model can be formulated and it is useful to consider how closely the assumptions must be satisfied for the model to be useful in understanding reality. To explore these questions exactly it would be necessary to establish more rigorous models. Time does not allow this and hence the discussion here is largely qualitative.

Assumption 1 restricts the model to perfect or nearly perfect similar folds. A variation in fold geometry as expressed by a variation in amplitude along the axial plane will remove the condition that differentiation with respect to y gives a zero result. In many natural folds the variation in amplitude along the axial plane is slight over distances comparable to the fold wavelength and the model is almost certainly applicable to these cases also.

The assumption of homogeneous anisotropic material to represent a multilayer sequence (assumption 2) is very good when fold wavelengths are long in relation to bed thickness, which is common in chevron folds (Ramsay 1974). This is because the bending resistance of competent units, neglected in the model, is less important at large wavelength to thickness ratios than small ratios. The bending resistance of the competent units will lessen the tendency to form sharp hinges at an early stage in the development of the folds and will also influence the mobility of the hinge.

Assumption 3, the use of linear viscous rheology in place of a power law behaviour, can be justified on the grounds that the deviatoric stress does not vary much across the fold profile. Hence a linearization represents a good approximation.

The assumption that the inflexion points are axes of two-fold rotational symmetry restricts the analysis to folds where this is approximately true.

Assumption 5, that the lines of inflexion points deform as passive markers was made as a matter of convenience and it could probably be justified by logical argument.

The proportion of natural folds satisfying the assumptions exactly is certainly very small. However natural folds satisfy the assumptions sufficiently closely for the model to provide a useful framework for understanding their development.

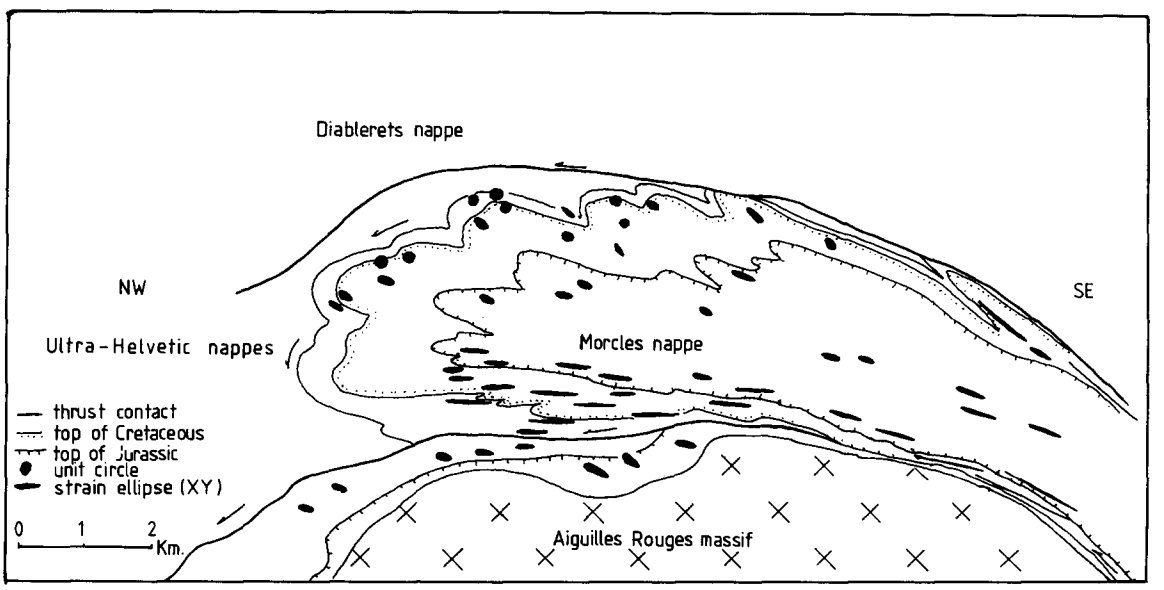

Fig. 6. Section through the Morcles Nappe showing strain measurements from naturally deformed objects and pressure shadows. Compilation of J. G. Ramsay from published and unpublished data of D. W. Durney, A. W. B. Siddans, D. Dietrich and J. G Ramsay (from Ramsay & Huber 1984).

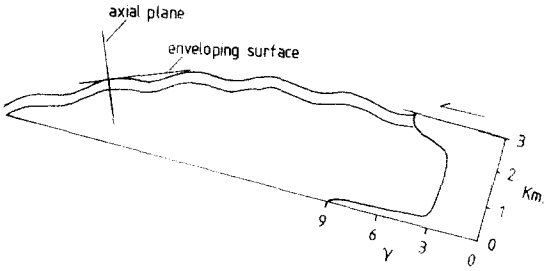

Fig. 7. Initial perturbation and simple-shear strain profile for the proposed model for the formation of the Morcles Nappe. The simple shear strain profile represents estimated finite values and not a simple shear rate profile.

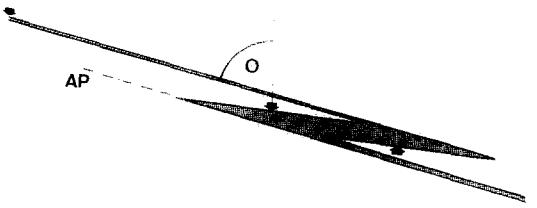

Fig. 9. Simulation of a fold from the overturned limb of the Morcles Nappe. The broad arrows mark the inflexion points. The initial amplitude to wavelength ratio was 0.01, the shear zone was at 10° to the enveloping surface of the initial perturbation and the anisotropy index m had a value of 0.01. The imposed simple shear strain was 12.8.

APPLICATION TO NATURAL FOLDS

To illustrate the application of the methods outlined above an attempt has been made to model the folds observed in the Morcles Nappe of the western Swiss Helvetic Nappes. The Morcles Nappe, shown in section with strain measurements in Fig. 6, is geometrically a large recumbent fold with smaller scale folds. Later uplift of the underlying Aiguilles Rouges massif has bowed the nappe upwards. The lower limb is very strongly deformed in what appears to be a shear zone. For the modelling of the folding in the nappe, the hypothesis that the structure developed by the imposition of heterogeneous simple shear deformation on an initial anticlinorium of low amplitude folds was adopted, (Fig. 7). It was assumed that the axial planes of the folds were initially perpendicular to the enveloping surface. The shear zone boundary is oblique to the enveloping surface except at the right hand side of the model, where the large-scale structure has its steepest dip to the right. The amount of simple shear imposed is greatest in the lower part of the nappe and falls off upwards except that towards the top it increases in value once more.

Simulations were carried out to discover how the folds might have developed in various parts of the nappe. Figure 8, taken from Badoux (1971), shows a fold on the highly deformed lower limb of the structure and a simulation is shown in Fig. 9. The overturned limb of the model fold is highly thinned relative to the normal limb. This compares well with the features seen in the natural folds. The vergence of the folds in nature and in the computer model is opposite to that which would be expected from the shear sense of the imposed deformation. This is a consequence of the fact that the shear zone is oblique to the enveloping surface of the initial folds. At high strains the line joining the inflexion points in the same horizon may be rotated through more than 90°. When this line passes the 90° position the relative lengths of the normal and overturned limbs reverses, so that below 90° the normal limb is longer and above 90° the overturned limb is the longer. The reversal takes place for $\gamma > \frac{1}{\tan\alpha}$ where α is the initial angle of the shear zone and the enveloping surface of the folds.

Figure 10 is a model of a fold from the upper part of the normal limb where the shear is again high. The initial angle of the shear zone and the enveloping surface was 5° which allows a large strain to be applied before the vergence changes. The fold form compares well with the fold towards the rear of the normal limb in Fig. 6.

A detailed study was made of folds from the frontal part of the nappe situated to the east of Pont de Nant (Swiss Cartographic Commission map coordinates 577,125/122,600). The folds occur in a multilayered sequence in the Argovian. Their wavelengths are of the order of 5–20 m. They are not minor folds of the first order in the nappe, but the axial planes and enveloping surfaces of the folds are parallel to those in the larger folds in the region. If it is assumed that the axial planes of the initial perturbations were originally at 90° to the enveloping surface, the amount of simple shear and the initial orientation of the shear zone can be estimated (see Fig. 11). The axial plane orientation before and after deformation gives the following equation for γ, (Ramsay 1967, equation 3–71)

$$\gamma = \cot\alpha - \cot(\alpha + \beta).$$

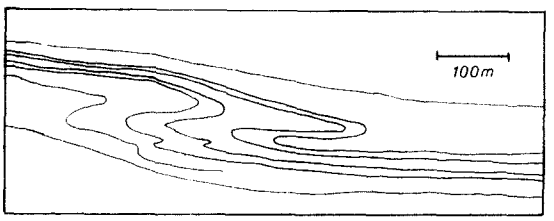

Fig. 8. A fold from the Malm limestones of the overturned limb of the Morcles nappe at La Tsantonnaire, looking eastwards. This fold is typical of the folds in the highly sheared region of the nappe, having a long inverted limb and a short normal limb. From Badoux (1971).

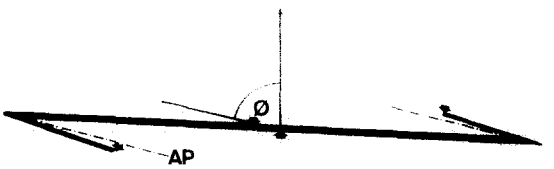

Fig. 10. Simulation of a fold from the top of the normal limb of the Morcles Nappe. The broad arrows mark the inflexion points. The initial amplitude to wavelength ratio was 0.01, the shear zone was at 5° to the enveloping surface of the initial perturbation and the anisotropy index was 0.001. The imposed shear strain was 6.8.

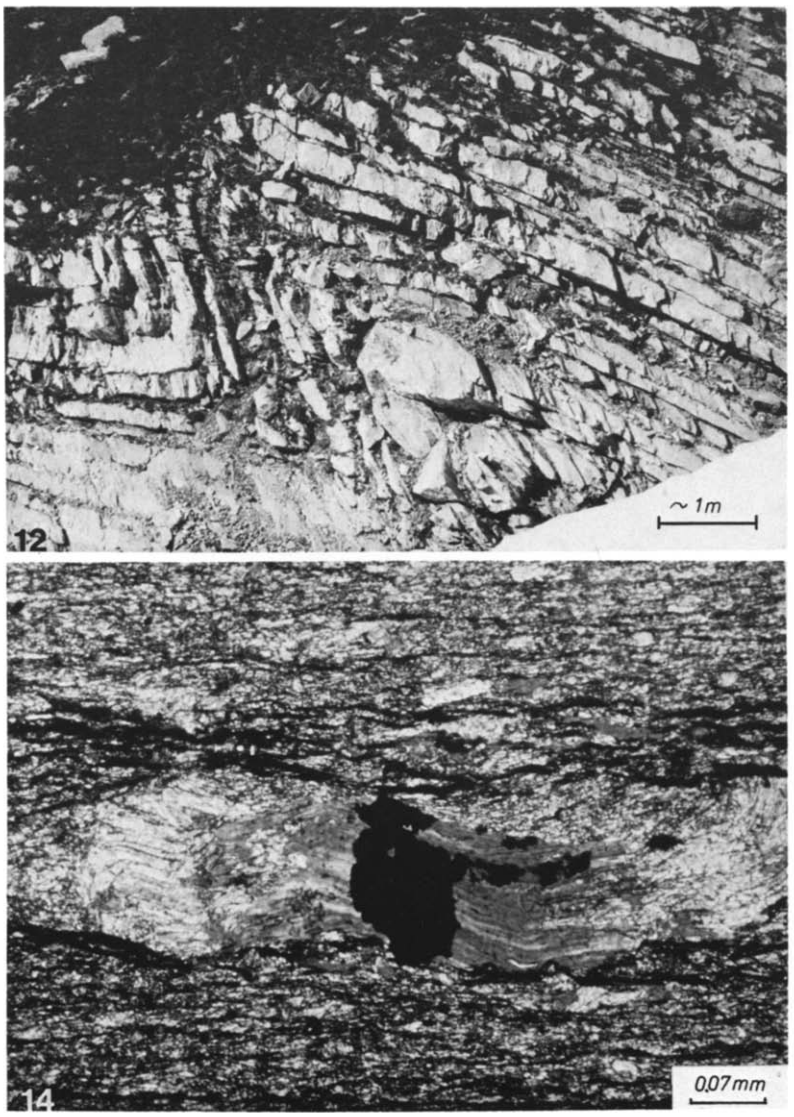

Fig. 12. The fold studied which is situated at Erbeuets, West of Pont de Nant. Swiss topographic map coordinates: 557,125/122,600.

Fig. 14. Example of a pressure shadow from one of the limestone units. The section was taken in the XZ section of the strain ellipsoid. The black horizontal lines in the photograph are the traces of pressure solution seams marking the cleavage.

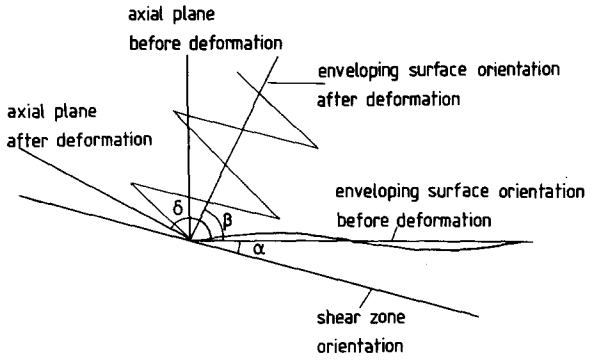

Fig. 11. Angular relationships of fold developing in simple shear. The assumptions of the theory allow the enveloping surface and axial plane to be treated as passive markers. It was assumed that the enveloping surface before deformation was horizontal.

The reorientation of the enveloping surface gives

$$\gamma = \cot(\alpha + 90°) - \cot(\alpha + \delta),$$

where α is the initial orientation of the enveloping surface, β is the final orientation of the enveloping surface and δ is the final orientation of the axial surface.

The above equations were solved graphically to give $\alpha = 12.5$ and $\gamma = 3.2$.

Figure 12 is a photograph showing the fold studied. The more competent units are limestones and the less competent units are marls. The hinge of the fold is very sharp and the limbs are straight. The folds are of similar type if surfaces in the same mechanical situation, such as the outer arcs of competent units, are considered. Cleavage is well developed in the less competent units and on each limb is within 5° of being parallel to the axial plane. In the more competent units the cleavage is less well developed and is refracted so as to form a convergent cleavage fan. The amount of refraction is approximately the same on each limb so that the cleavage is symmetric to the axial plane.

Both the competent and incompetent units have curved pressure shadows which allow deductions about the rotational components of the deformation to be made.

The fold profile resulting from a simulation with $\alpha = 12.5$, $m = 0.01$, $\gamma = 3.2$ and initial amplitude to wavelength ratio of 0.01 is shown in Fig. 13. Also shown in Fig. 13 are the orientations of the flattening plane of the finite strain ellipsoid calculated for the multilayers

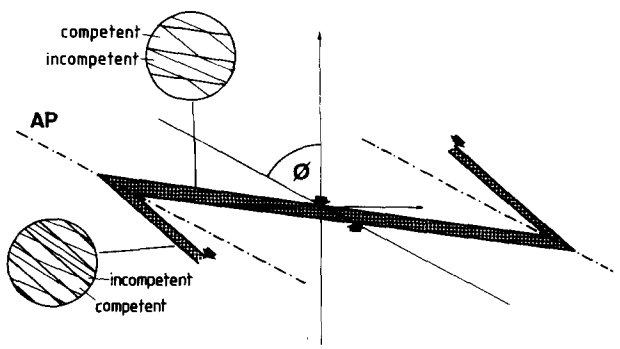

Fig. 13. Simulation of the fold shown in Fig. 12. The broad arrows mark the inflexion points.

Table 1. Bed thicknesses on each limb and their ratio. Mean value is 1.52 and the standard deviation is 0.31

Normal limb	Overturned limb	Ratio
1.5	1.2	1.25
2.1	1.7	1.24
2.4	1.2	2.00
0.75	0.5	1.50
1.3	0.8	1.62

on each fold limb. The multilayers had equal thickness components and the viscosity ratio was 0.4. The orientation of the flattening plane in the less competent unit in the model does not compare well with the orientation of the cleavage in the less competent unit of the natural example.

The values chosen for the parameters γ and α ensure that the orientation of axial planes and the enveloping surface and ratio of limb lengths are the same in the natural example and the model. The interlimb angle of the model, 34°, compares very well with that of the field example, 30°.

In Table 1 the bed thicknesses in each limb and their ratios are given. The mean ratio is 1.52 with a standard deviation of 0.32. The value given by the model is 1.55, which is within the standard deviation of the field measurements.

Pressure shadows were studied to obtain an indication of the deformation history at various points in the fold using the methods of Durney & Ramsay (1973). The samples came mostly from the competent limestone units, with only one from the incompetent material. The curvature of the fibres in the pressure shadows was found to be very consistent and is the same for both limbs. An example is shown in Fig. 14. The fibre geometry is a good indication that these folds formed in a rotational deformation. The analysis above shows that, when volume change is not considered, the instantaneous deformation at a point in the fold is a combination of the imposed bulk deformation and a heterogeneous simple shear. The latter component gives rise to the fold profile shape and has opposite senses on opposite limbs. When the imposed bulk deformation is simple shear it overwhelms any aspect of the heterogeneity in the simple shear strain field and the same type of deformation history results at all points in the fold. This is shown in Fig. 15, which is a plot of the rotation rate of the deformation in the competent units on each limb.

The following equation for anisotropy index m in terms of the thickness ratio F and viscosity ratio R was derived from equations for the shear and direct modulus given in Williams (1980, p.330)

$$m = \frac{R}{3(F + (1-F)R)(FR + 1 - F)}.$$

If F is set to 0.5 this equation can be rearranged to give a quadratic equation in R.

$$3mR^2 + (6m - 4)R + 3m = 0.$$

This gives $R \approx 1{,}331$ for $m = 0.001$ and $R \approx 131.3$ for $m = 0.01$.

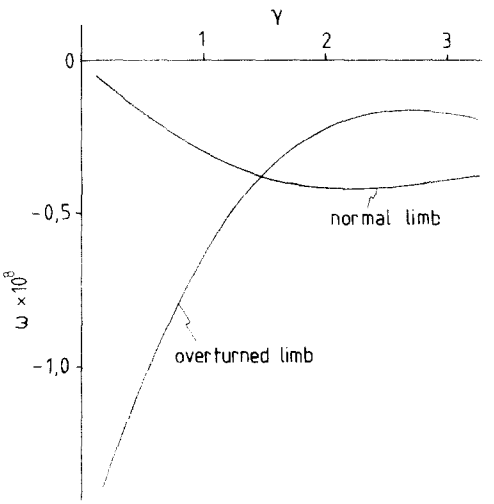

Fig. 15. Graph of the rigid rotation rate, ω, against γ for the more competent units of the simulation in Fig. 13.

These values are admittedly very high but knowledge of the rheology of marls is insufficient to rule out such values.

CONCLUSIONS

Using the similar fold model it is possible to simulate the finite geometry of folds in the Morcles Nappe.

The hypothesis that the Morcles Nappe formed by the heterogeneous simple shearing of a small initial perturbation is consistent with the observations.

For selected folds it was possible to vary the parameters of the model so that a good agreement was obtained for all geometric features of each fold; that is, the axial plane orientation, the enveloping surface orientation, the relation of cleavage to the axial plane, the interlimb angle and the relative thicknesses of the limbs.

The predictions of the model concerning deformation history, as expressed by the changes in the velocity gradient matrix, are consistent with observations of pressure shadows.

Acknowledgements—Financial support for both authors from Swiss Nationalfonds project no. 5.521.330.785/1 is gratefully acknowledged. Professor J. G. Ramsay is thanked for critical reading of the manuscript. Peter Cobbold and an anonymous referee are thanked for careful and constructive reviews of the manuscript.

REFERENCES

Badoux, H. 1971. Geologischer Atlas der Schweiz sheet 1305 Dt. de Morcles. Notice Explicative. Kümmerly & Frey, Bern.

Bayly, M. B. 1964. A theory of similar folding in viscous materials. *Am. J. Sci.* **262**, 753–766.

Biot, M. A. 1961. Theory of folding of stratified visco-elastic media and its implications in tectonics and orogenesis. *Bull. geol. Soc. Am.* **72**, 1305–1320.

Biot, M. A. 1965. *Mechanics of Incremental Deformations*. Wiley, New York.

Cobbold, P. R. 1976. Mechanical effects of anisotropy during large finite deformations. *Bull. Soc. géol. France* **18**, 1497–1510.

Cobbold, P. R., Cosgrove, J. W. & Summers, J. M. 1971. Development of internal structures in deformed anisotropic rocks. *Tectonophysics* **12**, 23–53.

Dieterich, J. H. 1969. Origin of cleavage in folded rocks. *Am. J. Sci.* **267**, 155–156.

Durney, D. W. & Ramsay, J. G. 1973. Incremental strains measured by syntectonic crystal growth. In: *Gravity and Tectonics* (edited by De Jong, K. A. & Scholten, R.). Wiley, New York, 67–96.

Eringen, A. C. 1962. *Nonlinear Theory of Continuous Media*. McGraw-Hill, New York.

Eringen, A. C. 1967. *Mechanics of Continua*. Wiley, New York.

Ralston, A. & Wilf, H. S. 1960. *Mathematical Methods for Digital Computers, Vol. 1*. Wiley, New York.

Ramberg, H. 1963. Fluid dynamics of viscous buckling, applicable to folding of layered rocks. *Bull. Am. Ass. Petrol. Geol.* **47**, 484–515.

Ramsay, J. G. 1967. *Folding and Fracturing of Rocks*. McGraw-Hill, New York.

Ramsay, J. G. 1974. Development of chevron folds. *Bull. geol. Soc. Am.* **85**, 1741–1754.

Ramsay, J. G. & Graham, R. H. 1970. Strain variation in shear belts. *Can. J. Earth. Sci.* **7**, 786–813.

Ramsay, J. G. & Huber, M. 1984. *The Techniques of Modern Structural Geology*. Academic Press, London.

Shimamoto, T. & Hara, I. 1976. Geometry and strain distribution of single layer folds. *Tectonophysics* **30**, 1–34.

Treagus, S. H. 1973. Buckling instability of a viscous single-layer system, oblique to the principal compression. *Tectonophysics* **19**, 271–289.

Williams, J. R. 1980. Similar and chevron folds in multilayers using finite-element and geometric models. *Tectonophysics* **65**, 323–338.

Zienkiewicz, O. C. 1971. *The Finite Element Method in Engineering Science*. McGraw-Hill, New York.